10-12-2020

Research and Simulation of DC Microgrid Three-Phase AC-DC Converter Control Strategy Based on Double Loop

Boning Wu
Tianjin University of Technology

Zhiqiang Gao
Cleveland State University, Z.GAO@csuohio.edu

Xuesong Zhou
Tianjin University of Technology, zxsmyj@126.com

Youjie Ma
Tianjin University of Technology, sjteam@163.com

Chenglong Wang
Tianjin Key Laboratory for Control Theory & Applications in Complicated Industry Systems

Research and Simulation of DC Microgrid Three-Phase AC-DC Converter Control Strategy Based on Double Loop

Boning Wu , Zhiqiang Gao ,Xuesong Zhou ,Youjie Ma ,Chenglong Wang

This work was supported in part by the National Natural Science Foundation of China under Grant 51877152 and in part by the Natural Science Foundation of Tianjin of China under Grant 18JCZDJC97300

ABSTRACT The new voltage and current double loop control strategy is proposed to solve the DC microgrid bus voltage fluctuation caused by loads fluctuation, parameters perturbation and unbalanced three-phase power supply. Firstly, the dq axis mathematical model of three-phase AC-DC bidirectional converter in DC microgrid is analyzed and established, and then the controllers are designed according to the dq axis mathematical model. The outer loop is a voltage loop based on variable gain linear extended state observer (VGLESO) and sliding mode theory. VGLESO can not only effectively overcome the problem of peak output of traditional high-gain LESO in the initial stage of operation, and ensure that the system has good startup characteristics, but also quickly track and compensate the total disturbance of the system without additional current sensors. The inner loop is a current loop based on adaptive PI, which can eliminate the influence of system parameters perturbation on bus voltage and improve the system's adaptability. Under the action of the inner and outer loops, the system has good dynamic and static characteristics. Finally, the feasibility and correctness of the control strategy are verified by Matlab/Simulink.

INDEX TERMS Adaptive PI, Bus voltage control, Dynamic characteristics, Feedforward control, Initial peak, Parameter perturbation, Variable gain linear extended state observer

I. INTRODUCTION

With the promotion and popularization of distributed energy grid connection and the increasingly strict requirements of users on the power quality of terminal power supply, the traditional AC distribution network gradually shows its deficiencies in the ability to accept new energy and power quality[1-3].

The circuit topology of a typical DC microgrid is shown in fig.1 Compared with the AC distribution network, the use number and frequency of power electronic devices of the DC microgrid are much smaller than that of the AC distribution network, which reduces the energy conversion link of the distributed power grid connection and the cost of grid connection. In addition, the DC microgrid does not need to track reactive power and phase, which improves the controllability of the system, the reliability of power supply and the economy of operation[4,5].

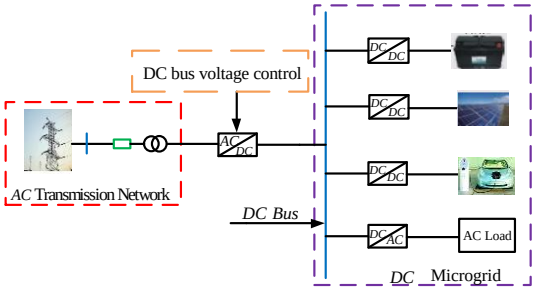

FIGURE 1. DC microgrid circuit topology

How to suppress the fluctuation of the bus voltage of the DC microgrid to ensure the stable operation of the system is one of the hot issues in the field of DC microgrid research. When the DC microgrid is connected to the AC power grid,

the control of the bus voltage is often achieved by optimizing the control system of the DC microgrid three-phase AC-DC bidirectional converter [6-8].However, the loads carried by the three-phase AC-DC bidirectional converter of the DC microgrid are usually complicated and changeable, that is, the external interferences are time-varying. Some parameters on the AC side of the converter, such as the equivalent resistance and inductance of the line, cannot be accurately measured. During use, these parameters often have different degrees of aging, and the parameters are perturbed. Therefore, in order to ensure that the converter tracks the reference signal quickly and accurately, the controller is required to have good dynamic and static characteristics and robustness to the time-varying loads and the perturbation of parameters.

At present, the control strategies of three-phase AC-DC converters in DC microgrids are mainly divided into linear and nonlinear control strategies. Among them, the linear control strategy is mainly based on linear PI, although PI control has been widely used in industry and achieved good control results. However, the PI controller based on the deviation control principle is difficult to overcome the control time lag caused by the capacitive element, which cannot meet the dynamic characteristics requirements of the power system [9, 10]. With the continuous development and improvement of the research on nonlinear control theory, nonlinear control strategies such as repetitive control, deadbeat control, fuzzy logic control, etc. have also been applied to different degrees in DC microgrids. Reference [11, 12] designed a repetitive controller for the three-phase AC-DC converter in DC microgrid, which improves the system's robustness to periodic disturbances. However, due to the inherent periodic delay of repetitive control, when the system is disturbed, at the moment, the control signal cannot act on the controlled object in time, which reduces the dynamic characteristics of the system. Reference [13-15] designed a fuzzy logic controller for power bidirectional AC-DC converter in DC microgrid, and applied it to the current inner loop in converter control system. This control strategy reduces the requirements for the mathematical model of the controlled object and improves the system's adaptability to the loads. But the realization of fuzzy logic control requires complex fuzzy operations, which increases the complexity of the system and construction costs.

Reference [16, 17] introduced current feedforward control strategy based on double-loop control for the three-phase AC-DC converter in DC microgrid, which significantly improved the dynamic characteristics of the system. However, the introduction of current feedforward requires additional current sensors, which will increase the construction and maintenance costs of the system. When there are multiple AC-DC converters in the bus, the selection of the sensor installation location will also become difficult.

Sliding mode control (SMC) not only has low requirements on the mathematical model of the system, but also has strong robustness to system parameters perturbation and external disturbances. Therefore, it is often used in non-linear systems, which are difficult to establish accurate mathematical models [18, 19]. However, in the traditional sliding mode control, a bigger control gain is required to improve the dynamic characteristics of the system, but excessive control gain and discontinuity of the control signal make the system have a certain degree of chattering, which seriously affects the engineering promotion of sliding mode control.

LESO, as the core of linear active disturbance rejection control (LADRC), has been well received by relevant practitioners since it was proposed. On the one hand, the number of parameters that LESO needs to be set is less, which reduces the difficulty of parameter setting and enhances the controllability of the system; On the other hand, LESO can also realize real-time tracking of state variables and total disturbance of the system when the controlled object mathematical model is unknown. Then, through the disturbance compensation link, the total disturbance of the system is approximately compensated, which solves the problem that the traditional current feedforward control needs additional sensors. Many experts and scholars have shown that the greater of the LESO error gain, the higher of the tracking accuracy[20, 21]. However, excessively large error gain will cause the "initial peak" problem in the initial stage of LESO operation, which will seriously affect the startup characteristics of the system.

Aimed at the "initial peak" problem of high gain LESO, this paper designs a variable gain linear extended state observer (VGLESO), whose gain is a time-varying function, and the gain coefficient is a very small value at the initial moment, with time, the gain coefficient gradually becomes a constant. On this basis, this paper, combining VGLESO with sliding mode theory, proposes a variable gain active disturbance sliding mode control strategy. And it is applied to the outer voltage loop of DC microgrid three-phase AC-DC converter control system. This control strategy not only preserves the structure of LESO feed-forward control, but also retains the strong robustness of sliding mode control. Last but not least, it also solves the problem of high gain LESO "initial peak" and the problem of traditional sliding mode control "chattering" caused by excessive gain. Detailed analysis will be carried out in the next chapter.

The *fal* function is a special non-linear structure, which is the mathematical fitting of "small error, large gain; large error, small gain" used for parameter adjustment of the control system[22]. According to the characteristic of the *fal* function, this paper uses it to correct the proportional integral gain of PI controller. And then, an adaptive PI control strategy is proposed to suppress the influence of the system parameter perturbation on the bus voltage.

Compared with the traditional double loop: in this paper, VGLESO and SMC are used to improve the voltage outer loop of three-phase AC-DC converter in DC microgrid. The current feedforward control with current signal as input is transformed into current feedforward control with voltage signal as input by VGLESO (The specific structure is shown in fig.3). This method can not only effectively suppress the initial peak value of LESO, but also effectively reduce the use of current sensors and reduce the cost of the device, at the same time, it also can reduce the chattering of sliding mode control; In this paper, the gain of the PI controller of the current inner loop is corrected by the nonlinear *fal* function to improve the system's adaptability to parameter perturbation(The specific structure is shown in fig.6). Finally, the feasibility of the control strategy proposed in this paper is verified by digital simulation.

The rest is of this paper organized as follows. Section II establishes the mathematical model of the DC microgrid three-phase AC-DC converter. Section III is the design of voltage outer loop based on VGLESO and sliding mode theory, including why to design VGLESO, how to design VGLESO, and the combination of VGLESO and sliding mode. Section IV is the design of current inner loop based on adaptive PI control strategy, including the description of nonlinear *fal* function characteristics, the design of current inner loop based on PI controller, and the combination of *fal* function and PI controller. Section V is the simulation. Section VI is the conclusion.

II. MATHEMATICAL MODEL OF DC MICROGRID AC-DC CONVERTER

The circuit topology of the three-phase AC-DC bidirectional converter of the DC microgrid is shown in fig. 2 In order to get a more concise mathematical expression of the AC-DC converter, combined with the actual power system, make the following assumptions:

a) The AC side power supply is an ideal three-phase power supply.

b) The AC system is a symmetrical three-phase system.

c) The power switch has no transition process, no power loss, and no dead zone.

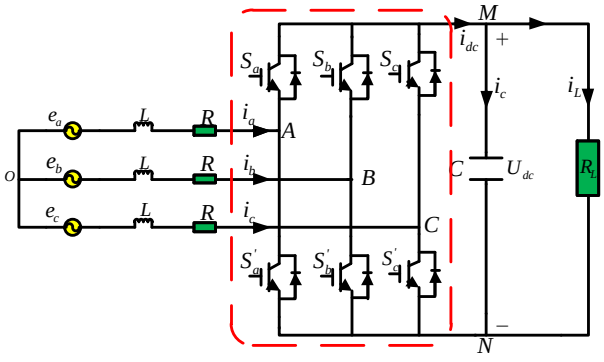

FIGURE 2. Topology diagram of converter in DC microgrid

In the picture: e_a, e_b, e_c is the equivalent three-phase AC power supply; i_a, i_b, i_c is the AC side line current; R is the line equivalent resistance; L is the line equivalent inductance; C is the DC side voltage stabilizing capacitor; U_{dc} is the voltage across the DC side capacitor; i_{dc} is DC current at both ends of the side; i_c is the current flowing through the ends of the capacitor; i_L is the current flowing through both ends of the load; R_L is the equivalent load of the DC microgrid; S_i is the switch function.

According to the circuit topology of the three-phase AC-DC converter of the DC microgrid, the mathematical model of the three-phase AC-DC bidirectional converter in the three-phase static coordinate system can be obtained by Kirchhoff's law. The AC side model is equation (1).

$$\begin{cases} L\dfrac{di_a}{dt} = e_a - Ri_a - (U_{dc}S_a - \dfrac{U_{dc}}{3}\sum\limits_{i=a,b,c} S_i) \\ L\dfrac{di_b}{dt} = e_b - Ri_b - (U_{dc}S_b - \dfrac{U_{dc}}{3}\sum\limits_{i=a,b,c} S_i) \\ L\dfrac{di_c}{dt} = e_c - Ri_c - (U_{dc}S_c - \dfrac{U_{dc}}{3}\sum\limits_{i=a,b,c} S_i) \end{cases} \tag{1}$$

The DC side model is equation (2).

$$C\frac{dU_{dc}}{dt} = i_a S_a + i_b S_b + i_c S_c - i_L \tag{2}$$

In the above equation:

$$S_i = \begin{cases} 1, & i \text{ phase upper swith is on} \\ 0, & i \text{ phase bottom swith is on} \end{cases} \quad i = a,b,c \tag{3}$$

The current on the AC side is nonlinear and strongly coupled, it is not conducive to the design of the controller. Therefore, in order to simplify the controller design, it is necessary to use coordinate transformation to change the three-phase stationary coordinate system into a two-phase rotating coordinate system.

The transformation matrix from the three-phase stationary coordinate system to the two-phase stationary coordinate system is equation (4).

$$C_{3s/2s} = \frac{2}{3}\begin{bmatrix} 1 & -\dfrac{1}{2} & -\dfrac{1}{2} \\ 0 & \dfrac{\sqrt{3}}{2} & -\dfrac{\sqrt{3}}{2} \end{bmatrix} \tag{4}$$

The transformation matrix from the two-phase stationary coordinate system to the two-phase rotating coordinate system is equation (5).

$$C_{2s/2r} = \begin{bmatrix} \cos\theta & \sin\theta \\ -\sin\theta & \cos\theta \end{bmatrix} \tag{5}$$

In the above equation: θ is the angle that the d -axis leads the a -axis.

The mathematical model of three-phase AC-DC converter in two-dimensional rotating coordinate system can be obtained by simultaneous equation (1-5).

$$\begin{cases} L\dfrac{di_d}{dt} = e_d - Ri_d - U_{dc}S_d + \omega Li_q \\ L\dfrac{di_q}{dt} = e_q - Ri_q - U_{dc}S_q - \omega Li_d \end{cases} \tag{6}$$

$$C\frac{dU_{dc}}{dt} = \frac{3}{2}(S_d i_d + S_q i_q) - i_L \tag{7}$$

Both sides of equation (7) take derivatives of time at the same time, and then combine equation (6) to get equation (8).

$$\begin{aligned} \frac{d^2U_{dc}}{dt^2} = {} & \frac{3}{2LC}\sum_{k=d,q}(S_k e_k - S_k i_k R) - \frac{3}{2LC}\sum_{k=d,q}(S_k U_k) \\ & + \frac{3\omega}{2C}S_d i_q - \frac{1}{C}\dot{i}_L - \frac{3\omega}{2C}S_q i_d \end{aligned} \tag{8}$$

In the above equation: e_d , e_q are the components of the AC side voltage vector of the three-phase AC-DC converter on the axis of the rotating coordinate system; i_d , i_q are the components of the AC side current vector of the three-phase AC-DC converter on the axis of the rotating coordinate system; S_d , S_q are the components of the AC side switching function of the three-phase AC-DC converter on the axis of the rotating coordinate system.

From equation (8), we can see that the AC-DC bidirectional converter in the DC microgrid can be regarded as a second-order system. For a measurable second-order system, the state variable and total disturbance of the system can be observed by designing an appropriate linear expansion state observer.

III. DESIGN OF VOLTAGE OUTER LOOP BASED ON VGLESO AND SLIDING MODE THEORY

As the core of linear active disturbance rejection control, LESO can not only track the state variables in the system in real time, but also approximate the total disturbance of the system. Then, the system can be approximately compensated through the disturbance compensation link, which is equivalent to the structure of the feedforward control system. It can significantly improve the dynamic characteristics of the system. High gain LESO has the problem of "peak output" at the initial stage of operation, which seriously affects the start-up performance of the system. In order to solve this problem, this paper designs VGLESO, which can effectively solve the problem of "initial peak" of LESO, and improve the start-up characteristics of the system.

Sliding mode control, as a kind of nonlinear control, has low requirements on the mathematical model of the controlled object and strong robustness to load changes. In the actual implementation of sliding mode control, it is often necessary to set a larger sliding mode coefficient to improve the dynamic characteristics of the system. However, an excessively large sliding mode coefficient will further amplify the discontinuity of sliding mode control, resulting in high-frequency "chattering" of the system, which seriously affects the practical engineering application of sliding mode control.

In order to simplify the design of sliding mode control and solve the "chattering" problem of sliding mode control, this paper combines VGLESO and sliding mode control theory to the design of voltage outer loop in three-phase AC-DC converter control system. VGLESO can track all state variables in the system, which are applied to design the sliding mode controller. In addition, VGLESO can estimate the total disturbance of the system, that are approximately compensated through the disturbance compensation link. This will reduce the sliding mode coefficient, slows down the pressure of sliding mode controller and suppresses the "chattering" of sliding mode control.

A. CONTRADICTION ANALYISIS OF LESO OBSERVATION ACCURACY AND INITIAL PEAKING PHENOMENON

For a second-order nonlinear system:

$$\ddot{x}_1 = f(x_1, \dot{x}_1, w(t)) + (b - b_0)u(t) + b_0 u(t) \tag{9}$$

In the above equation: $x_1, \dot{x}_1, \ddot{x}_1$ are the state variable of the system; $f(x_1, \dot{x}_1, w(t)) + (b - b_0)u(t)$ is the total disturbance of the system; $w(t)$ is the external disturbance of the system; $u(t)$ is the control variable of the system; b is the control gain of the system, b_0 is the approximate value of b ; $y = x_1$ is the output of the system.

Let $\dot{x}_1 = x_2$, $\dot{x}_2 = x_3 + b_0 u(t)$, $x_3 = f(x_1, \dot{x}_1, w(t)) + (b - b_0)u(t)$. In the modeling process of low-frequency three-phase AC-DC converters, the switching function is often described by the duty cycle, so it can be regarded as a small constant. In practical control systems, $u(t)$ is differentiable. Therefore, x_3 is differentiable. let $\dot{x}_3 = f$ .Then the expanded system can be described as equation (10).

$$\begin{cases} \dot{x}_1 = x_2 \\ \dot{x}_2 = x_3 + b_0 u(t) \\ \dot{x}_3 = f \\ y = x_1 \end{cases} \tag{10}$$

The corresponding third-order LESO is equation (11).

$$\begin{cases} e(t) = z_1(t) - x_1(t) \\ \dot{z}_1 = z_2(t) - a_1 e(t) \\ \dot{z}_2 = z_3(t) - a_2 e(t) + b_0 u(t) \\ \dot{z}_3 = -a_3 e(t) \end{cases} \tag{11}$$

In the above equation: $z_1(t)$ 、 $z_2(t)$ and $z_3(t)$ are the state variables of the expanded state observer, a_1 、 a_2 and a_3 are all greater than zero, which is the error feedback gain of the expanded state observer.

Known by equation (11):

$$\begin{cases} z_1(t) = x_1(t) + e(t) \\ z_2(t) = \dot{z}_1 + a_1 e(t) \\ z_3(t) = \dot{z}_2 + a_2 e(t) - b_0 u(t) \end{cases} \tag{12}$$

Further sorting equation (12) can get equation (13).

$$\begin{cases} z_1(t) = x_1(t) + e(t) \\ z_2(t) = x_2(t) + a_1 e(t) + \dot{e}(t) \\ z_3(t) = x_3(t) + a_2 e(t) + a_1 \dot{e}(t) + \ddot{e}(t) \end{cases} \tag{13}$$

From equation (13), we can see that LESO adjusts the change of the observed value according to the deviation signal of the observed value and the actual value, so as to realize the tracking of the system state variables. From the tracking process of state variables, LESO should firstly complete the tracking of $z_1(t)$ to $x_1(t)$, secondly complete the tracking of $z_2(t)$ to $x_2(t)$, and finally complete the tracking of $z_3(t)$ to $x_3(t)$. Although the tracking of each state variable is performed at the same time, the order of completion of tracking should be like this. Before the adjustment of $z_1(t)$ is completed, the adjustment of $z_2(t)$ and $z_3(t)$ to track their respective actual values cannot be completed. When $z_1(t)$ finishes tracking $x_1(t)$, it becomes difficult to track $x_2(t)$ and $x_3(t)$. The reason is that the value of $e(t)$ is very small at this time. In order to enable LESO to continue tracking $z_2(t)$ to $x_2(t)$ and $z_3(t)$ to $x_3(t)$, a_2 and a_3 need to be set to a larger value. It can be seen from equation (13) that an excessively large error gain coefficient will intensify the peak output phenomenon of LESO at the initial time ($e(t)$、 $\dot{e}(t)$ and $\ddot{e}(t)$ are inherent characteristics of the system and cannot be changed). This leads to the contradiction between the high gain LESO tracking accuracy and the initial peak is not adjustable[23].

B. VGLESO DESIGN

In order to effectively solve the problem of high-gain LESO output peak value at the initial moment, this paper designed a VGLESO, the specific expression of which is shown in the following equation.

$$\begin{cases} e(t) = z_1(t) - x_1(t) \\ \dot{z}_1 = z_2(t) - a_1 e(t) \\ \dot{z}_2 = z_3(t) - a_2 \beta_2(t) e(t) + b_0 u(t) \\ \dot{z}_3 = -a_3 \beta_3(t) e(t) \end{cases} \tag{14}$$

In the above equation:

$$\beta_i(t) = \begin{cases} (b_i t)^{n_i}, & 0 \le t < \dfrac{1}{b_i} \\ 1, & \dfrac{1}{b_i} \le t \end{cases} \qquad i = 2,3 \tag{15}$$

In the above equation: b_i is used to limit the value of time t; n_i is used to limit the unevenness and degree of unevenness of the function; 1 is to ensure that the parameters a_1、 a_2、 a_3 are consistent with the parameters of high gain LESO. $\beta_i(t)$ makes VGLESO not only effectively suppress the initial peak phenomenon, but also maintain the high-precision tracking performance of traditional high-gain LESO.

The traditional high-gain LESO error feedback gain selection method is usually to use pole placement[24].

The characteristic equation of equation (11) is equation (16).

$$s^3 + a_1 s^2 + a_2 s + a_3 = 0 \tag{16}$$

In order to obtain a good tracking effect, the pole of the characteristic equation is usually placed at the bandwidth of the observer.

$$s^3 + a_1 s^2 + a_2 s + a_3 = (s + \omega_0)^3 \tag{17}$$

In the above equation: ω_0 is the bandwidth of the linearly expanded state observer

According to the nature of the identity, expand equation (17) to get equation (18):

$$\begin{cases} a_1 = 3\omega_0 \\ a_2 = 3\omega_0^2 \\ a_3 = \omega_0^3 \end{cases} \tag{18}$$

As a result, the original configuration problem of LESO parameters was transformed into the selection of LESO bandwidth, which reduced the difficulty of parameter adjustment.

C. PROOF OF CONVERGENCE OF VGLESO

For the VGLESO convenience of proof, change equation (14) to equation (19).

$$\begin{cases} e(t) = z_1(t) - x_1(t) \\ \dot{z}_1 = z_2(t) - h_1 e(t) \\ \dot{z}_2 = z_3(t) - h_2(t) e(t) + b_0 u(t) \\ \dot{z}_3 = -h_3(t) e(t) \end{cases} \tag{19}$$

In the above equation:

$$\begin{cases} h_1 = a_1 \\ h_2(t) = a_2 \beta_2(t) \\ h_3(t) = a_3 \beta_3(t) \end{cases} \tag{20}$$

Let:

$$\begin{cases} e_1(t) = z_1(t) - x_1(t) \\ e_2(t) = z_2(t) - x_2(t) \\ e_3(t) = z_3(t) - x_3(t) \end{cases} \tag{21}$$

Equation (22) can be get by equations (19-21).

$$\begin{cases} \dot{e}_1(t) = e_2(t) - h_1 e_1(t) \\ \dot{e}_2(t) = e_3(t) - h_2(t) e_1(t) \\ \dot{e}_3(t) = -h_3(t) e_1(t) - f \end{cases} \tag{22}$$

Let:

$$\begin{cases} X_1 = e_1(t) \\ X_2 = e_2(t) - h_1 e_1(t) \\ X_3 = e_3(t) - h_1 e_2(t) - (h_2(t) - h_1^2) e_1(t) \end{cases} \tag{23}$$

Thus, the error state equation of variable gain LESO can be obtained.

$$\begin{cases} \dot{X}_1 = X_2 \\ \dot{X}_2 = X_3 \\ \dot{X}_3 = -h_1 X_3 - h_2(t) X_2 - (\dot{h}_2(t) + h_3(t)) X_1 - f \end{cases} \tag{24}$$

The characteristic equation of equation (24) is equation (25).

$$s^3 + h_1 s^2 + h_2(t)s + \dot{h}_2(t) + h_3(t) = 0 \tag{25}$$

According to the Horwitz stability criterion, equation (25) only needs to meet the conditions($\Delta_1 > 0, \Delta_2 > 0, \Delta_3 > 0$) , that the system is asymptotically stable at a large range at the equilibrium point($e_1(t) = 0,\ e_2(t) = 0,\ e_3(t) = 0$),which means that VGLESO can track the system state variables and disturbances well.

$$\begin{cases} \Delta_1 = h_1 > 0 \\ \Delta_2 = \begin{vmatrix} h_1 & 1 \\ \dot{h}_2(t) + h_3(t) & h_2(t) \end{vmatrix} = h_1 h_2(t) - \dot{h}_2(t) - h_3(t) > 0 \\ \Delta_3 = \begin{vmatrix} h_1 & 1 & 0 \\ \dot{h}_2(t) + h_3(t) & h_2(t) & h_1 \\ 0 & 0 & \dot{h}_2(t) + h_3(t) \end{vmatrix} = (\dot{h}_2(t) + h_3(t))\Delta_2 > 0 \end{cases} \tag{26}$$

D. DESIGN OF SLIDING MODE CONTROLLER BASED ON VGLESO

In order to obtain a good control effect, the voltage error of the DC bus and the differential signal of the voltage error are selected as the state variables of the sliding mode function.

Select the sliding mode function as the following equation:

$$s = ce + \dot{e} \tag{27}$$

According to the Horwitz stability criterion, if c is greater than zero, the system (27) is asymptotically stable in a large range.

In the above equation:

$$\begin{cases} e = U_{dcr} - U_{dc} \\ \dot{e} = \dot{U}_{dcr} - \dot{U}_{dc} \end{cases} \tag{28}$$

In the above equation: U_{dcr} is the rated value of bus voltage and U_{dc} is the real-time value of bus voltage.

Take derivative of $\dot{e}$ again to get equation (29).

$$\ddot{e} = \ddot{U}_{dcr} - \ddot{U}_{dc} \tag{29}$$

According to equation (8), the AC-DC bidirectional converter of the DC microgrid can be equivalent to a second-order system. For an observable second-order system, the state variable and total disturbance can be tracked and observed through the system (14). The specific tracking method is as follows.

$$\begin{cases} \lim\limits_{t\to\infty} z_1 = U_{dc} \\ \lim\limits_{t\to\infty} z_2 = \dot{U}_{dc} \\ \lim\limits_{t\to\infty} z_3 = \ddot{U}_{dc} - b_0 u \end{cases} \tag{30}$$

In order to effectively suppress chattering and ensure that the system state variables can reach the sliding mode surface within a limited time, this paper uses an exponential approach rate to design the sliding mode controller. The specific form is shown by the following equation:

$$\dot{s} = -\varepsilon sign(s) - ks \tag{31}$$

In the above equation: $\varepsilon > 0$, $k > 0$ 。 ε is the speed at which the system state variable tends to the sliding mode surface. If the value of ε is too small, the system will take a long time to reach the sliding mode surface from the initial state. And the dynamic characteristic of the system is very poor. If the value of ε is too large, it will cause chattering of the system, which is not conducive to the stability of the system. k is the coefficient of the exponential approach term. The larger the k value, the better the dynamic characteristics of the system. But if the value of k is too large, it will aggravate the chattering of the system[25, 26].

The control rate of the system can be obtained by simultaneous equation (27-31).

$$u = b_0^{-1}(\varepsilon sign(s) + ks - cz_2 - z_3) \tag{32}$$

On the one hand, VGLESO overcomes the "initial peak" phenomenon of high-gain LESO, ensures that the system has a high tracking accuracy at the initial stage. On the other hand, the state variables s, z_2, z_3 in equation (32) extraction can be achieved through VGLESO, which greatly reduces the number of actual system sensors used. Finally, from equation (32), we can see that the disturbance compensation part is added to the control rate u , which greatly reduces the sliding mode coefficient and suppresses system chatter.

Figure 3 shows three-phase AC-DC voltage outer loop of DC microgrid based on VGLESO and sliding mode theory.

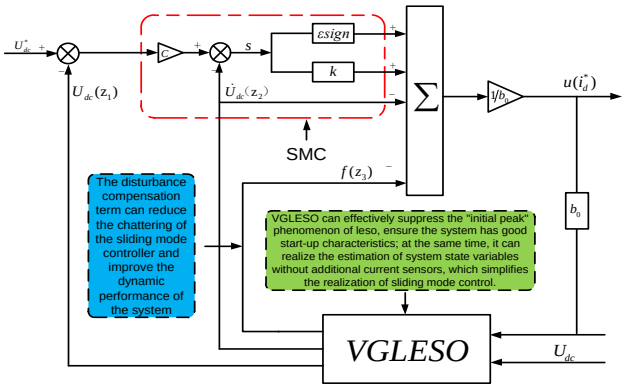

FIGURE 3. **Voltage outer loop controller**

IV. DESIGN OF CURRENT INNER LOOP BASED ON ADAPTIVE PI CONTROLLER

As a typical control strategy, PI controller has been widely used in modern control systems because of its good control effects, simple designs and easy engineering implementation. But in the actual control systems, once the parameters of PI controller are set, it is difficult to be changed again. When the parameters of the system are perturbed, the original gain of PI controller is not the optimal control gain of the system. Therefore, as for those systems whose parameters are easily perturbed, PI control is difficult to achieve good control effect. *fal* function is a special nonlinear structure, which is the mathematical fitting of "small error, large gain; large error, small gain" used in parameter adjustment of control system. Combined with the characteristics of the *fal* function, this article uses the *fal* function to correct the

control gains of the PI controller to improve the adaptability of the PI controller. Then an adaptive PI control strategy is proposed and applied to the current inner loop in the DC microgrid three-phase AC-DC converter control system.

A. INTRODUCTION OF ADAPTIVE PI CONTROLLER

The mathematical expression of the *fal* function is as follows:

$$fal(e,\ \alpha,\ \delta)=\begin{cases}|e|^{\alpha}\,sign(e), & |e|\geq\delta\\ \dfrac{e}{\delta^{1-\alpha}}, & |e|<\delta\end{cases} \tag{33}$$

In the above equation: δ is the length of the linear region; α is the exponential term coefficient, which is a constant between (0-1), and determines the degree of nonlinearity of the function and the rate of increase of the function; e is the deviation signal of the system state variable.

In order to reflect the characteristics of the *fal* function more intuitively, a *fal* function model was built in Matlab/Simulink. The unit ramp function is used as input, keeping α=0.5 unchanged, δ taking different values, and observing the effect of δ change on the function value of *fal* function. The output result is shown in fig.4 (Because the *fal* function is an odd function, only the function image in the first quadrant is studied here. Same as below)

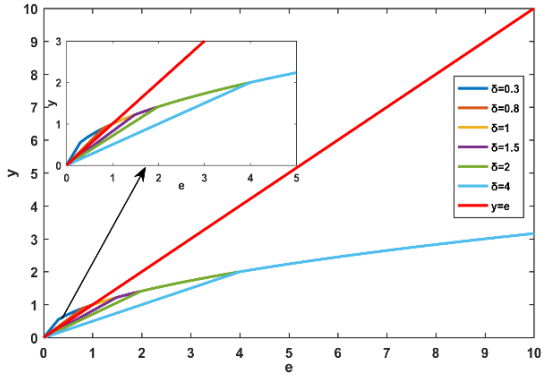

FIGURE 4. **Function output image corresponding to different δ**

The unit ramp function is used as input, keeping the parameter $\delta=0.5$ unchanged, α taking different values, and observing the effect of α change on the *fal* function. The output waveform is shown in fig.5.

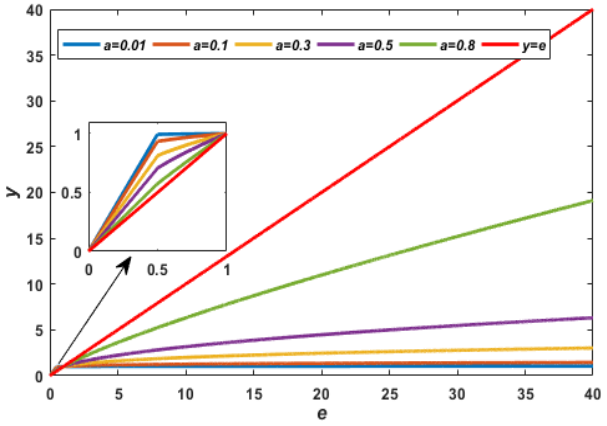

FIGURE 5. **Function output image corresponding to different α**

It can be seen from fig.4 that the value of δ not only determines the length of the linear region of the *fal* function, but also determines whether the slope of the *fal* function in the range of $(0,\delta)$ is greater than 1. Therefore, when the deviation signal is the input of the controller, the feedback gain can be corrected by adjusting the δ parameter of the *fal* function. This can ensure that when the deviation signal is small, the gain of PI controller is larger (more than the linear gain), so that the system has better control accuracy and efficiency.

Combining equation (33) and fig.5, we can see that the curve has changed at $\delta=0.5$. The curve is linear in the range of $\delta<0.5$.And the curve is non-linear in the range of $\delta\geq0.5$. The degree of nonlinearity of the curve is inversely related to the value of α . Therefore, when the deviation signal of the state variable is used as the input of the controller, the feedback gain can be corrected by adjusting the α parameter of the *fal* function. When the state variable deviation signal is large, the gain of the PI controller is small; When the state variable deviation signal is small, the gain of the PI controller is large. This can ensure that the PI controller has good adaptability to the system load parameter perturbation.

In conclusion, the control law of the adaptive PI controller is equation (34).

$$u_0=k_p\,fal(e,\alpha_p,\delta_p)+k_i\,fal(e,\alpha_i,\delta_i) \tag{34}$$

In the above equation: k_p is the proportional gain, k_i is the differential gain.

The structure of adaptive PI controller based on *fal* function is shown in fig.6.

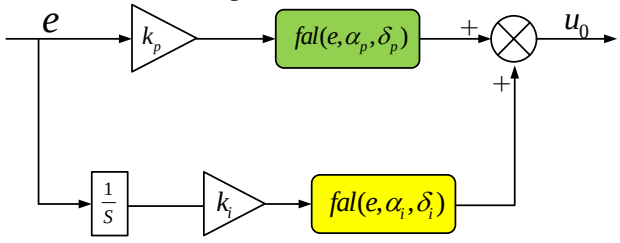

FIGURE 6. **Adaptive PI controller based on *fal* function**

B. DESIGN OF CURRENT INNER LOOP BASED ON TRADITIONAL PI CONTROLLER

The mathematical model of the DC microgrid three-phase AC-DC converter in the two-dimensional rotating coordinate system is equation (6).

Let:

$$\begin{cases} U_d = S_d U_{dc} \\ U_q = S_q U_{dc} \end{cases} \tag{35}$$

In the equation: U_d is the output variable of the d-axis of the current inner loop; U_q is the output variable of the q-axis of the current inner loop; S_d and S_q are the corresponding components of the switch function $S_i (i = a,b,c)$ in the two-dimensional rotating coordinate system. U_{dc} is the DC microgrid bus voltage.

Equation (36) can be obtained by combining equations (6) and (35).

$$\begin{cases} U_d = -L\dfrac{di_d}{dt} - Ri_d + e_d + \omega L i_q \\ U_q = -L\dfrac{di_q}{dt} - Ri_q + e_q - \omega L i_d \end{cases} \tag{36}$$

In the above equation: i_d and i_q are the corresponding current component of i_a, i_b, i_c in the two-dimensional rotating coordinate system; e_d and e_q are the corresponding voltage components of the voltage vectors U_a, U_b, U_c in the two-dimensional rotating coordinate system; ω is the rotation angular frequency of the AC grid; L is the line equivalent inductance; R is the line equivalent resistance.

In the initial state of zero, the Laplace transform is taken on both sides of equation (36) at the same time, and the frequency domain equation of the three-phase AC-DC bidirectional converter in the two-phase rotating coordinate system is obtained.

$$\begin{cases} U_d(s) = -LsI_d(s) - RI_d(s) + e_d(s) + \omega L I_q(s) \\ U_q(s) = -LsI_q(s) - RI_q(s) + e_q(s) - \omega L I_d(s) \end{cases} \tag{37}$$

In the above equation: $I_d(s)$ is the Laplace transform of i_d; $I_q(s)$ is the Laplace transform of i_q; $e_d(s)$ is the Laplace transform of e_d; $e_q(s)$ is the Laplace transform of e_q; $U_d(s)$ is the Laplace transform of U_d; $U_q(s)$ is the Laplace transform of U_q.

Equation (38) can be obtained by sorting out equation (37).

$$\begin{cases} e_d(s) - U_d(s) + \omega L I_q(s) = (Ls + R) I_d(s) \\ e_q(s) - U_q(s) - \omega L I_d(s) = (Ls + R) I_q(s) \end{cases} \tag{38}$$

According to equations (37) (38), we can see that in the two-dimensional rotating coordinate system, the output variable $U_d(s)$, $U_q(s)$ and the input variable $I_q(s)$, $I_d(s)$ of the system are coupled. It is difficult to design a controller for a coupled system. Thus, it is necessary to take a feedforward decoupling method to achieve decoupling control between dq axis state variables. The specific decoupling method is given in APPENDIX C.

After complete decoupling, when PI control strategy is adopted in the current inner loop of the three-phase AC-DC converter control system, the output equation of the controller can be obtained.

$$\begin{cases} U_d(s) = -(k_{pd} + \dfrac{k_{id}}{s})(I_d^*(s) - I_d(s)) + e_d(s) + \omega L I_q(s) \\ U_q(s) = -(k_{pq} + \dfrac{k_{iq}}{s})(I_q^*(s) - I_q(s)) + e_q(s) - \omega L I_d(s) \end{cases} \tag{39}$$

Equation (40) can be obtained by substituting equation (39) into equation (37).

$$\begin{cases} (Ls + R) I_d(s) = (k_{pd} + \dfrac{k_{id}}{s})(I_d^*(s) - I_d(s)) \\ (Ls + R) I_q(s) = (k_{pq} + \dfrac{k_{iq}}{s})(I_q^*(s) - I_q(s)) \end{cases} \tag{40}$$

In the above equation: k_{pd} is the d-axis proportional gain; k_{pq} is the q-axis proportional gain; k_{id} is the d-axis integral gain; k_{iq} is the q-axis integral gain; $I_d^*(s)$ is the d-axis current inner loop reference value; $I_q^*(s)$ is the q-axis current inner loop reference value.

C. CONTRADICTION ANALYSIS BETWEEN OPTIMAL PARATTER SETTING OF PI CONTROLLER AND PARATTER PERTURBATION OF SYSTEM

Since the two current inner loops in dq coordinate system are symmetrical, so only the design of d-axis current inner loop is given to be an example for analysis. Considering the sampling delay of signal and the small inertia characteristic of PWM control, the current inner loop control block diagram is shown in fig.7.

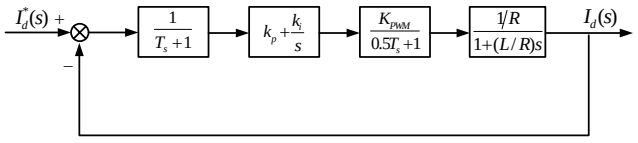

FIGURE 7. Current inner loop control block diagram Schematic

In fig.7: T_s is the current sampling period; K_{PWM} is the equivalent gain of the converter PWM control system.

In order to reduce the difficulty of parameter setting of PI controller, the small time constant T_s is combined with $0.5T_s$. Rewrite the transfer function of the PI controller to the pole-zero form, which is showed in equation (41). The simplified current inner loop control block diagram can be obtained, as shown in fig.8.

$$k_p + \frac{k_i}{s} = k_p(\frac{\tau_i s + 1}{\tau_i s}) \tag{41}$$

In the above equation: τ_i is the integral time constant, $k_i = k_p / \tau_i$.

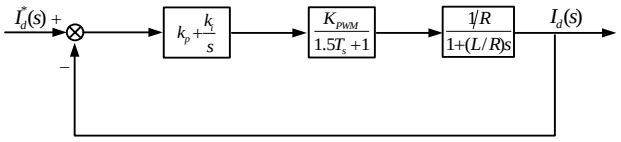

FIGURE 8. Simplified current inner loop control block diagram

In order to ensure that the current inner loop has good tracking characteristic, the parameters of the PI controller are set according to a typical I system. It can be seen from fig.8, if the zero point of the PI controller is used to cancel the pole of the controlled object's transfer function, that is, let $\tau_i = L/R$ .The open-loop transfer function of the current inner loop can be obtained, which is designed according to the typical I-type system.

The corrected open-loop transfer function of the current inner loop is equation (42).

$$G_0(s) = \frac{k_p K_{PWM}}{R\tau_i s(1.5T_s s+1)} \tag{42}$$

The open-loop transfer function of a typical type I system is equation (43).

$$G_i(s) = \frac{\omega_n^2}{s(s+2\xi\omega_n)} \tag{43}$$

In the above equation: $G_i(s)$ is the open-loop transfer function of the standard I system; ω_n is the angular frequency of natural oscillation; ξ is the damping ratio.

When the damping ratio is equal to $\sqrt{2}/2$, equation (44) can be obtained by simultaneous equations (42) and (43).

$$\frac{1.5T_s k_p K_{PWM}}{L} = \frac{1}{2} \tag{44}$$

The proportional and integral gains can be obtained by equation (44).

$$\begin{cases} k_p = \dfrac{L}{3T_s K_{PWM}} \\ k_i = \dfrac{R}{3T_s K_{PWM}} \end{cases} \tag{45}$$

According to equation (45), once the system parameters R and L are determined, the optimal control gain of the system will be determined. It's hard to be changed again, when k_p and k_i are set. Therefore, when the system parameters (R , L) are perturbed, the previously control gain will no longer be the optimal control gain. It will reduce the dynamic characteristics of power system and affect the reliability of power supply. So it is necessary to adopt an adaptive PI controller to solve this problem.

D. DESIGN OF CURRENT INNER LOOP BASED ON ADAPTIVE PI

For the problems mentioned in section ***C***, the PI controller gain can be corrected by the *fal* function introduced in section ***A***. The specific implementation way is shown in equation (46).

$$\begin{cases} U_d(s) = -(k_{pd}\, fal_{pd} + \dfrac{k_{id}\, fal_{id}}{s})(I_d^*(s) - I_d(s)) + e_d(s) + \omega L I_q(s) \\ U_q(s) = -(k_{pq}\, fal_{pq} + \dfrac{k_{iq}\, fal_{iq}}{s})(I_q^*(s) - I_q(s)) + e_q(s) - \omega L I_d(s) \end{cases} \tag{46}$$

In the above equation: fal_{pd} is the d -axis proportional gain correction function; fal_{id} is the d -axis integral gain correction function; fal_{pq} is the q -axis proportional gain correction function; fal_{iq} is the q -axis integral gain correction function.

V. SIMULATION AND ANALYSIS

In order to test the suppression effect of VGLESO on the "initial peak" and verify the control effect of the control strategy proposed in this paper, the DC microgrid shown in fig.9 was built in Matlab/Simulink. In the simulation program, the sampling period is 0.00005s, the limiting link is [-450,450]. System parameters and controller parameters are shown in APPENDIX A and APPENDIX B.

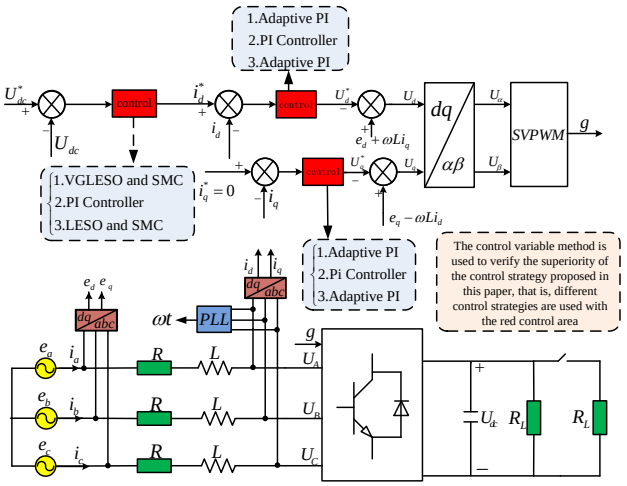

FIGURE 9. DC microgrid

A. VGLESO INHIBITORY EFFCT ON LESO INITIAL PEAK

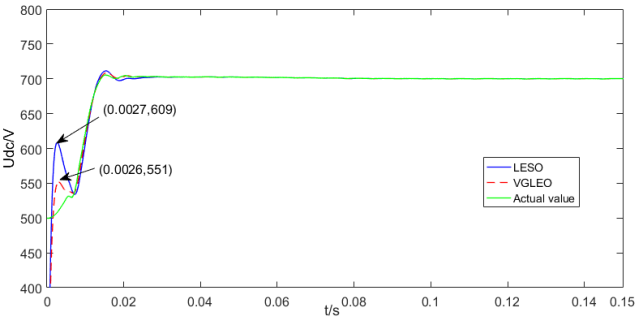

FIGURE 10. Tracking curve of state variable x_1 (U_{dc})

Figure 10 shows the tracking curves of VGLESO and traditional high gain LESO to the system state variable U_{dc} . It can be seen from the figure that under the premise of

ensuring the same tracking accuracy, VGLESO effectively weakens the initial peak of high gain LESO.

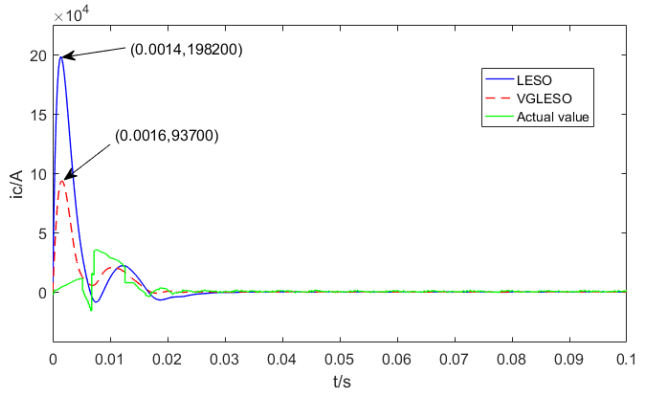

FIGURE 11. Tracking curve of state variable x_2 (i_c)

It is not conducive to measure the value of the state variable $\dot{U}_{dc}$ .Because the $\dot{U}_{dc}$ has no clear physical meaning. Thus, the state variable $\dot{U}_{dc}$ is converted into a current i_c flowing through the two ends of the capacitor. According to equation (46), we know that the value size of i_c reflects the change of $\dot{U}_{dc}$. As can be seen from fig.11, the initial peak value of VGLESO is about half of that of LESO.

$$C\dot{U}_{dc} = i_c \tag{46}$$

B. STUDY ON SYSTEM START-UP CHARACTERISTICS

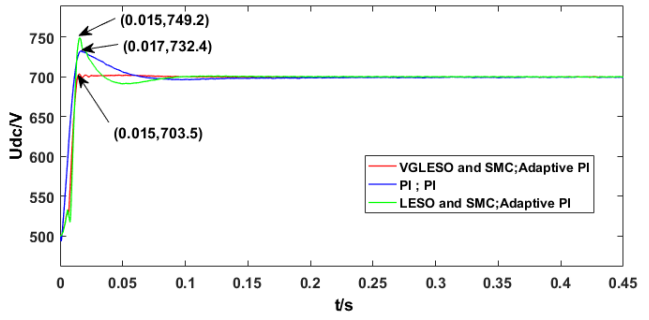

FIGURE 12. Starting characteristics

Figure 12 shows the waveform of bus voltage when bidirectional AC-DC converter is started with different control strategies. It can be seen from the figure that, on the one hand, the rise time of the system under the control of the two controllers is the same, but the overshoot of the two controllers is quite different. Among them, the overshoot of the system under the control of VGLESO and SMC is almost zero, while the overshoot of the system under the control of LESO and SMC is 7%. On the other hand, when the bus voltage reaches the rated voltage 700V, the system under the control of VGLESO and SMC is basically maintained near the rated voltage, almost no transient process, while the system under the control of LESO and SMC needs a series of transition processes to maintain near the rated voltage. In conclusion, the start-up performance based on VGLESO and SMC controller is better than that based on LESO and SMC controller.

C. STUDY ON THE INFLUENCE OF THE VOLTAGE FLUCTUATION OF THE BUS WHEN THE LOAD ON THE DC SIDE SUDDENLY REDUCES BY HALF

In order to study the influence of sudden load halving on bus voltage, the simulation experiments under two conditions are carried out.

a) Condition 1: The system operates stably before 0.5s. At 0.5s, the resistive load is suddenly halved, and the bus voltage fluctuation diagram is shown in fig.13.

b) Condition 2: The system operates stably before 0.9s. At 0.9s, the constant power load is suddenly halved, and the bus voltage fluctuation diagram is shown in fig.14.

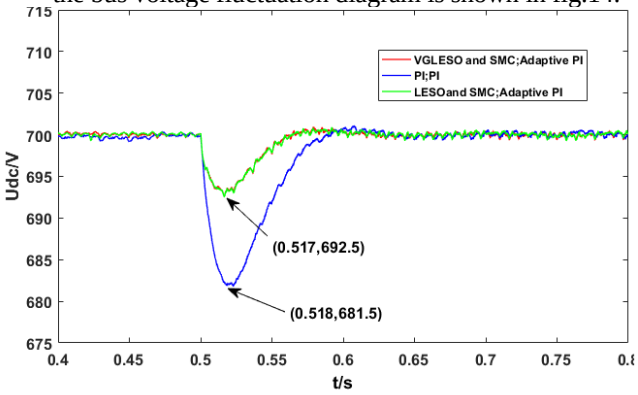

FIGURE 13. Voltage fluctuation diagram of resistance load suddenly halved

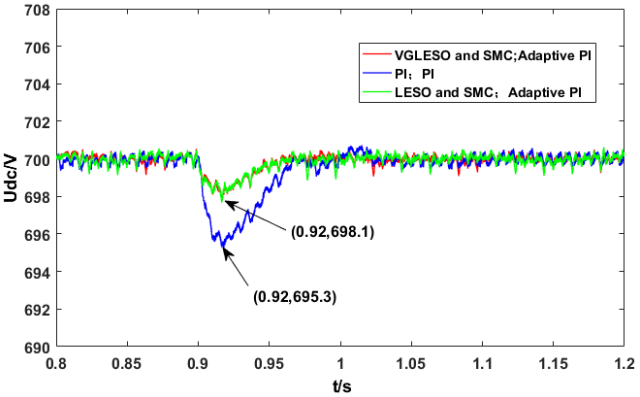

FIGURE 14. Voltage fluctuation diagram of bus with sudden half reduction of constant power rate load

When the load current suddenly decreases, since the voltage across the capacitor cannot be abrupt, the change of the current i_{dc} on the DC side lags behind the change of the load current i_L .So the current i_c flowing across the capacitor should be reduced. According to equation (47), the bus voltage will drop.

$$\Delta U_{dc} = \frac{1}{C}\int_{t_0}^{t} \Delta i_c dt \tag{47}$$

It can be seen from fig.13 and fig.14 that the control performance of VGLESO and SMC is now consistent with the control effect of LESO and SMC, and the transition process time and voltage oscillation range of both are smaller than PI control strategy. Therefore, the control strategy

proposed in this paper can suppress the voltage fluctuation of DC bus and shorten the transition time of the system.

D. STUDY ON THE INFLUENCE OF PARAMETER FLUCTURTION ON BUS VOLTAGE

In order to study the control effect of the adaptive PI controller, two groups of parameter perturbations under different operating conditions are implemented in Matlab / Simulink.

a) Condition 1: The system is stable before 1.3s. At 1.3s, the equivalent load of phase a line suddenly increases from 1 Ω to 3 Ω. At 1.5s, the parameter perturbation disappears and the AC system becomes a balanced three-phase system. The bus voltage fluctuation diagram is shown in fig.15 (a).

b) Condition 2: The system operates stably before 2.6s. At 2.6s, the equivalent load of phase a line suddenly decreases from 1 Ω to 0.1 Ω; at 2.8s, the equivalent load of phase B and C lines also drops to 0.1 Ω. The bus voltage fluctuation diagram is shown in fig.15(b).

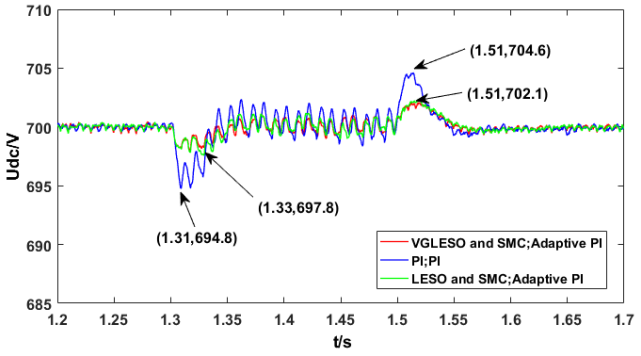

(a)

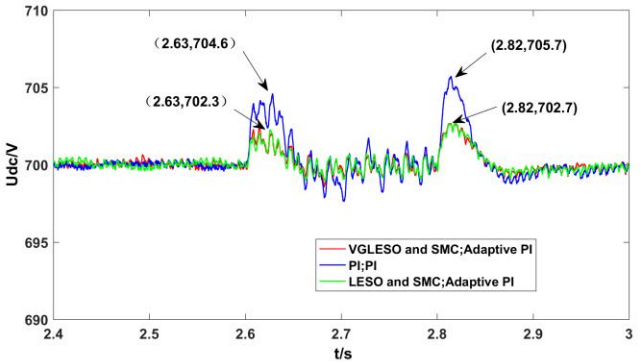

(b)

FIGURE 15. Voltage fluctuation diagram of parameter perturbation bus(a) Parameter increase(b) Parameter reduction

It can be seen from fig.17 (a) (b) that when the system parameters are disturbed, compared with PI controller, the overshoot of adaptive PI controller is smaller (the drop is smaller), and the transition time is shorter .When the system reaches the steady state again, the system voltage fluctuation under the control of the adaptive PI controller is smaller and the steady state characteristic is better. In conclusion, the adaptive PI controller has stronger adaptability to system parameter perturbation.

E. STUDY ON THE INFLUENCE OF AC SIDE VOLTAGE DROP ON BUS VOLTAGE

In order to study the low voltage ride through capability of the control strategy proposed in this paper, the following experiments are carried out in Matlab / Simulink. At 3.3s, the voltage at the AC side suddenly drops by 50% with a duration of 0.2s. fig.16 shows the three-phase voltage waveform, and fig.17 shows the corresponding DC bus voltage waveform.

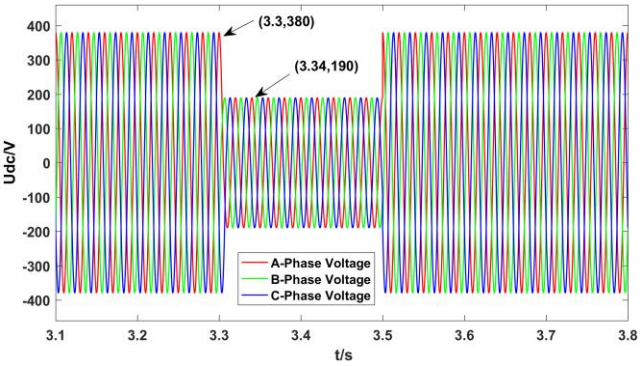

FIGURE 16. Three phase voltage waveform

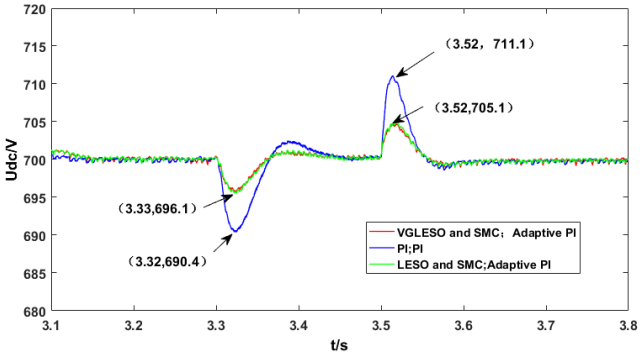

FIGURE 17. DC bus voltage waveform

It can be seen from fig.17 that when the voltage drops, the bus voltage dropping amplitude of the control strategy proposed in this paper is about half of that of PI controller. When the voltage recovers, the voltage overshoot of the control strategy proposed in this paper is about half of that of PI controller. To sum up, the control strategy proposed in this paper has stronger ability of low voltage ride through

VI. CONCLUSION

Aiming at the mathematical model of AC-DC converter in DC microgrid, considering the initial peak value of high gain LESO, a VGLESO is designed to track and estimate the state variables and total disturbances of the system. And the convergence of the VGLESO is proved. On this basis, the variable gain active disturbance rejection sliding mode control strategy is designed by combining the sliding mode theory with VGLESO. In addition, aiming at the problem that the traditional PI controller is too sensitive to the system parameter perturbation, the adaptive PI control law based on the *fal* function is designed.

The simulation results show that, compared with the high gain LESO, the VGLESO designed in this paper can not effectively weaken the initial peak phenomenon, but also maintain the high observation accuracy of the high gain LESO. The control strategy based on VGLESO and sliding mode theory can realize the feedforward control without additional current sensors, which improves the dynamic quality of the control system. At the same time, compared with the traditional linear PI controller, the adaptive PI controller can overcome the influence of parameter perturbation on the bus voltage. Finally, because the design of the two controllers does not depend on the structure and parameters of the system, they have strong robustness and portability, especially for the nonlinear system which is difficult to establish accurate mathematical model.

Although VGLESO weakens the output peak of LESO at the initial moment and enhances its engineering practicability, its parameter designs are based on the working experience of researchers. It is not conducive for the large-scale industrial promotion of this technology. Therefore, the next work of the author is to give the parameter setting criteria of VGLESO.

APPENDIX A

TABLE I
SYSTEM PARAMETERS

Symbol	Quantity	Value
V	phase voltage	$380\,V$
f	voltage source frequency	$50\,Hz$
R	line equivalent resistance	$1\,\Omega$
L	line equivalent inductance	$0.01\,H$
C	DC side capacitance	$0.08\,F$
V	Initial voltage of DC side capacitance	$500\,V$
R_r	DC side resistive load	$40\,\Omega$
R_p	DC side power load	$3000\,W$

APPENDIX B

TABLE II
CONTROLLER PARAMETERS

Symbol	Quantity	Value
c	Sliding Mode Controller	110
k	Sliding Mode Controller	182
ε	Sliding Mode Controller	100
ω_0	Observer Bandwidth	495
b_0	Control gain	19625
b_2	VGLESO parameters	300
b_3	VGLESO parameters	500
n_2	VGLESO parameters	0.31
n_3	VGLESO parameters	0.8
k_{pd}	Inner Loop PI Controller Parameters	20
k_{id}	Inner Loop PI Controller Parameters	120
k_{pq}	Inner Loop PI Controller Parameters	20
k_{iq}	Inner Loop PI Controller Parameters	120
δ_p	*fal* function parameter	0.8
α_p	*fal* function parameter	0.682
δ_d	*fal* function parameter	0.75
α_d	*fal* function parameter	0.95

APPENDIX C

The feed-forward variables $-\omega LI_q(s)$ and $\omega LI_d(s)$ are introduced into the output of the AC voltage of the three-phase converter to cancel the items with $\omega LI_q(s)$ and $-\omega LI_d(s)$ in the converter structure, which realizes the decoupling between the dq axis state variables. After decoupling, the structure of the system is transformed into two independent parts, as shown in fig.(1).

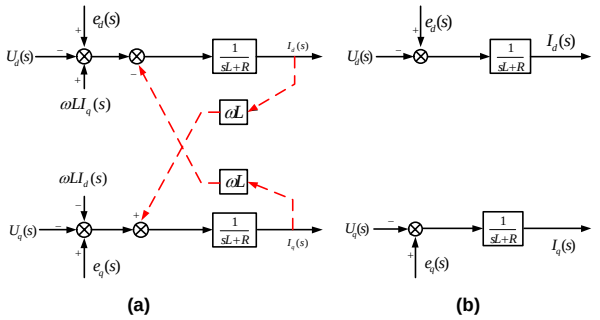

FIGURE (1). Feedforward decoupling control of three-phase AC-DC converter (a) Feedforward decoupling diagram of three-phase AC-DC converter (b) Equivalent model of three-phase AC-DC converter after feedforward decoupling

It can be seen from (b) in fig.(1) that although the feedforward compensation realizes decoupling of state variables of d-axis and q-axis, it does not realize complete decoupling. Because the value of $I_d(s)$ is not only influenced by $U_d(s)$, but also by $e_d(s)$.Therefore, there is coupling between $I_d(s)$ and $e_d(s)$,which is detrimental to the design of the controller.For this reason, it is necessary to adopt the feedforward decoupling strategy again to achieve the decoupling of $I_d(s)$ and $e_d(s)$.The specific implementation method is that $-e_d(s)$ is introduced into the AC output side of the three-phase AC-DC converter to cancel the $e_d(s)$ in the converter structure, so as to realize the decoupling of $I_d(s)$ and $e_d(s)$ (The analysis of the q-axis is similar to that of the d-axis, so it is not repeated here.) The structure diagram of the system before and after decoupling is shown in fig.(2).

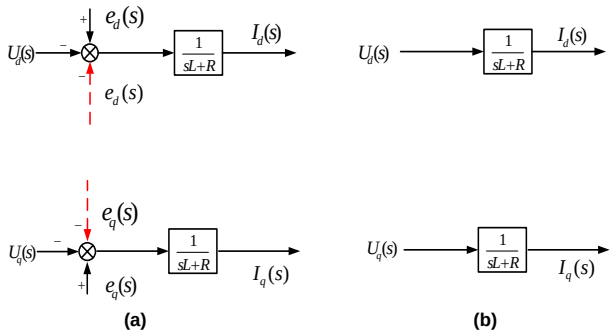

FIGURE (2). Single-axis feedforward decoupling control of three-phase AC-DC converter (a) Single axis feedforward decoupling diagram of three-phase AC-DC converter (b) Equivalent model of three-phase AC-DC converter after single-axis feedforward decoupling

According to equation (39), after twice feedforward decoupling controls, the grid-side d -axis frequency domain equation of the three-phase AC-DC converter contains only the d -axis component, which realizes complete decoupling. This makes the design of the PI controller easier and the system more stable. The schematic diagram of current decoupling control is shown in fig. (3).

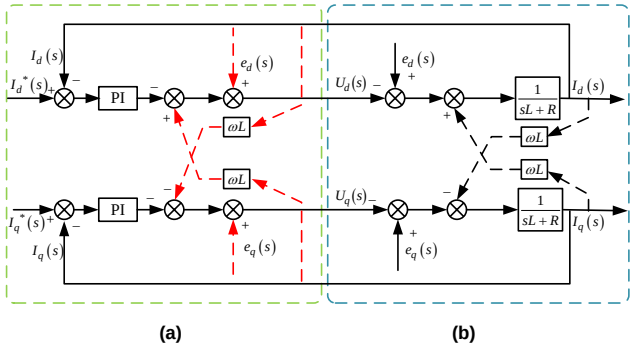

FIGURE (3). Schematic diagram of current decoupling control (a) Block diagram of current decoupling control based on PI controller (b) The dq mathematical model of three-phase AC-DC converter

REFERENCES

[1] S. Gao, S. Liu, Y. Liu, X. Zhao, and T. E. Song, "Flexible and Economic Dispatching of AC/DC Distribution Networks Considering Uncertainty of Wind Power," Ieee Access, vol. 7, pp. 100051-100065, 2019, 2019.

[2] J. Duan, Z. Li, Y. Zhou, and Z. Wei, "Study on the voltage level sequence of future urban DC distribution network in China: A Review," *International Journal of Electrical Power & Energy Systems*, vol. 117, May, 2020.

[3] J. Barros, M. de Apraiz, and R. I. Diego, "Power Quality in DC Distribution Networks," *Energies*, vol. 12, no. 5, Mar 1, 2019.

[4] Y. Li, L. He, F. Liu, C. Li, Y. Cao, and M. Shahidehpour, "Flexible Voltage Control Strategy Considering Distributed Energy Storages for DC Distribution Network," *Ieee Transactions on Smart Grid*, vol. 10, no. 1, pp. 163-172, Jan, 2019.

[5] J. M. Guerrero, A. Davoudi, F. Aminifar, J. Jatskevich, and H. Kakigano, "Guest Editorial: Special Section on Smart DC Distribution Systems," *Ieee Transactions on Smart Grid*, vol. 5, no. 5, pp. 2473-2475, Sep, 2014.

[6] Y. Liu, H. Li, Z. Yu, and R. Zeng, "Reliability evaluation method for AC/DC hybrid distribution power network considering cascaded multiport power electronic transformer," *Iet Generation Transmission & Distribution*, vol. 13, no. 23, pp. 5357-5364, Dec 3, 2019.

[7] M. Llomplat, J. E. Bosso, R. E. Carballo, and G. O. J. I. P. E. Garcia, "Novel modified phase-shift modulation strategy for isolated AC–DC power converters," vol. 13, no. 5, pp. 1022-1032, 2020.

[8] R. K. Chauhan, K. Chauhan, J. M. J. J. o. R. Guerrero, and S. Energy, "Controller design and stability analysis of grid connected DC microgrid," vol. 10, no. 3, pp. 035101, 2018.

[9] M. Shi, X. Chen, J. Zhou, Y. Chen, J. Wen, and H. He, "Distributed Optimal Control of Energy Storages in a DC Microgrid With Communication Delay," *Ieee Transactions on Smart Grid*, vol. 11, no. 3, pp. 2033-2042, May, 2020.

[10] R. Hemalatha, and M. Ramasamy, "Microprocessor and PI controller based three phase CHBMLI based DSTATCOM for THD mitigation using hybrid control techniques," *Microprocessors and Microsystems*, vol. 76, Jul, 2020.

[11] M. Tang, S. Bifaretti, S. Pipolo, S. Odhano, and P. Zanchetta, "A Novel Repetitive Controller Assisted Phase-Locked Loop with Self-Learning Disturbance Rejection Capability for Three-Phase Grids," *Ieee Journal of Emerging and Selected Topics in Power Electronics*, vol. 8, no. 2, pp. 1870-1879, Jun, 2020.

[12] G. A. Ramos, R. I. Ruget, and R. Costa-Castello, "Robust Repetitive Control of Power Inverters for Standalone Operation in DG Systems," *Ieee Transactions on Energy Conversion*, vol. 35, no. 1, pp. 237-247, Mar, 2020.

[13] S. Bayhan, S. Demirbas, and H. J. I. R. P. G. Aburub, "Fuzzy-PI-based sensorless frequency and voltage controller for doubly fed induction generator connected to a DC microgrid," vol. 10, no. 8, pp. 1069-1077, 2016.

[14] F. Qu, J. Liu, H. Zhu, and D. Zang, "Wind Turbine Condition Monitoring Based on Assembled Multidimensional Membership Functions Using Fuzzy Inference System," *Ieee Transactions on Industrial Informatics*, vol. 16, no. 6, pp. 4028-4037, Jun, 2020.

[15] W. C. de Carvalho, R. P. Bataglioli, R. A. S. Fernandes, and D. V. Coury, "Fuzzy-based approach for power smoothing of a full-converter wind turbine generator using a supercapacitor energy storage," *Electric Power Systems Research*, vol. 184, Jul, 2020.

[16] C. Zhang, X. Wang, P. Lin, P. X. Liu, Y. Yan, and J. Yang, "Finite-Time Feedforward Decoupling and Precise Decentralized Control for DC Microgrids Towards Large-Signal Stability," *Ieee Transactions on Smart Grid*, vol. 11, no. 1, pp. 391-402, Jan, 2020.

[17] W. Jiang, S. Xue, L. Zhang, W. Xu, K. Yu, W. Chen, and L. Zhang, "Flexible Power Distribution Control in an Asymmetrical-Cascaded-Multilevel-Converter-Based Hybrid Energy Storage System," *Ieee Transactions on Industrial Electronics*, vol. 65, no. 8, pp. 6150-6159, Aug, 2018.

[18] A. Levant, "Higher-order sliding modes, differentiation and output-feedback control," *International Journal of Control*, vol. 76, no. 9-10, pp. 924-941, Jun-Jul, 2003.

[19] A. Levant, "Robust exact differentiation via sliding mode technique," *Automatica*, vol. 34, no. 3, pp. 379-384, Mar, 1998.

[20] X. Wang, R. Liao, C. Shi, and S. Wang, "Linear Extended State Observer-Based Motion Synchronization Control for Hybrid Actuation System of More Electric Aircraft," *Sensors*, vol. 17, no. 11, Nov, 2017.

[21] P. Liu, Z. Zheng, S. Chen, W. Sun, and Z. Sun, "Continuous momentum management for space station based on LESO," *Aerospace Science and Technology*, vol. 72, pp. 364-370, Jan, 2018.

[22] D. Wu, and K. Chen, "Frequency-Domain Analysis of Nonlinear Active Disturbance Rejection Control via the Describing Function Method," *Ieee Transactions on Industrial Electronics*, vol. 60, no. 9, pp. 3906-3914, Sep, 2013.

[23] C. Jing, H. Xu, X. Song, and B. Lu, "Adaptive extended state observer-based flatness nonlinear output control for torque tracking of electrohydraulic loading system," *Transactions of the Institute of Measurement and Control*, vol. 40, no. 10, pp. 2999-3009, Jun, 2018.

[24] Q. Zheng, Z. Chen, and Z. Gao, "A practical approach to disturbance decoupling control," *Control Engineering Practice*, vol. 17, no. 9, pp. 1016-1025, Sep, 2009.

[25] Y. Wei, J. H. Park, H. R. Karimi, Y.-C. Tian, and H. Jung, "Improved Stability and Stabilization Results for Stochastic Synchronization of Continuous-Time Semi-Markovian Jump Neural Networks With Time-Varying Delay," *Ieee Transactions on Neural*

Networks and Learning Systems, vol. 29, no. 6, pp. 2488-2501, Jun, 2018.

[26] Y. Liu, Z. Wang, L. Xiong, J. Wang, X. Jiang, G. Bai, R. Li, and S. Liu, "DFIG wind turbine sliding mode control with exponential reaching law under variable wind speed," *International Journal of Electrical Power & Energy Systems*, vol. 96, pp. 253-260, Mar, 2018.